
UV-Net: Learning from Curve-Networks and Solids

Pradeep Kumar Jayaraman*
Autodesk Research

Aditya Sanghi
Autodesk Research

Joseph Lambourne
Autodesk Research

Thomas Davies
Autodesk Fusion 360

Hooman Shayani
Autodesk Research

Nigel Morris
Autodesk Research

Abstract

Parametric curves, surfaces and boundary representations are the basis for 2D vector graphics and 3D industrial designs. Despite their prevalence, there exists limited research on applying modern deep neural networks directly to such representations. The unique challenges in working with such representations arise from the combination of continuous non-Euclidean geometry domain and discrete topology, as well as a lack of labeled datasets, benchmarks and baseline models. In this paper, we propose a unified representation for parametric curve-networks and solids by exploiting the u- and uv-parameter domains of curve and surfaces, respectively, to model the geometry, and an adjacency graph to explicitly model the topology. This leads to a unique and efficient network architecture based on coupled image and graph convolutional neural networks to extract features from curve-networks and solids. Inspired by the MNIST image dataset, we create and publish WireMNIST (for 2D curve-networks) and SolidMNIST (for 3D solids), two related labeled datasets depicting alphabets to encourage future research in this area. We demonstrate the effectiveness of our method using supervised and self-supervised tasks on our new datasets, as well as the publicly available ABC dataset. The results demonstrate the effectiveness of our representation and provide a competitive baseline for learning tasks involving curve-networks and solids.

1 Introduction

An important requirement for designing shapes on computers is the ability to create visually pleasing curves and surfaces in a representation that is accurate and concise while being easy to modify by casual users and designers alike. Parametric curves and surfaces are the basis for a huge portion of designs done on computers. In 2D, a connected set of parametric curves such as lines, arcs, or more generally quadratic and cubic Bézier curves are used in designing fonts, layout plans, and freehand drawings, and natively supported by popular formats such as the Scalable Vector Graphics (SVG). In 3D, parametric surfaces such as planes, cylinders, cones, spheres and toroids, Non-Uniform Rational B-Splines (NURBS), and T-splines [22] are the building blocks for designing freeform and solid models. Patches of such geometry are stitched together using a boundary representation (B-rep) [29, 18], which is composed of faces (bounded portions of surfaces), edges (bounded pieces of curves) and vertices (points).

Despite parametric curves, surfaces and boundary representations being the industry standard for 2D and 3D design, there exists limited research on applying deep neural networks directly to such representations. The challenges in feeding such data to neural networks lie in the input representation: First, parametric representations of shapes are not unique,

*Email: {pradeep.kumar.jayaraman, aditya.sanghi, joseph.lambourne, thomas.davies, hooman.shayani, nigel.morris}@autodesk.com

hence one cannot feed raw data such as spline control points into a neural network, since the same shape can be represented by many parameterizations. Therefore, the representation has to preferably be invariant to a particular parametrization for most applications. Second, a wide range of primitives and freeform parametric curves and surfaces, each with their own set of parameters, need to be considered. Third, the ordering of data e.g., control points in spline representations, is important. Fourth, even if we tackle all the above challenges, we still need to consider how different curve and surface elements are put together to form the entire shape, i.e. the topology. This is particularly challenging with the B-rep data structure which is complex, and allows different representations for the same shape, e.g. merging faces 1 and 2 in the inset figure.



Indeed, the combination of continuous non-Euclidean geometry [4] and discrete topology is uniquely challenging compared to previous representations considered in the deep learning literature such as images and voxel-grid representations of 3D shapes. A straightforward approach for feature extraction from parametric representations, is to preprocess them into well-studied representations, like images, voxels, point clouds, signed-distance functions, and triangle meshes which are ubiquitous in deep learning literature. Although plausible, such conversions are neither differentiable, nor trivial, and generally not favorable due to the following reasons: First, it is difficult to reconstruct a solid back since it requires reverse engineering with careful regularizations to get a smooth shape. Furthermore, since a single surface is often not sufficient to represent the entire shape, we also need a good segmentation of points/triangles, and fit a surface for each of the segments, which is a hard, ill-posed problem. Second, discrete representations such as pointclouds or voxels suffer from loss of fidelity and can miss small faces unless the sampling/tessellation is very dense, and generally do not scale well with the complexity of the shape.

Given these challenges, a natural research direction is to explore the design of input representations as well as neural network models that will enable feature extraction from parametric spline models. This can enable us to leverage massive digital design data which already exists in such formats today for various applications ranging from classification, shape retrieval to eventually generating new designs. However, there is no standardized way for modern neural networks to consume B-reps. In this paper, we take a step in this direction and make the following contributions:

- We present a new unified representation of curve-networks and solid models, which captures geometric features by considering the parameter domain as a regular grid, and encapsulate the topological features in the adjacency information of a graph. This representation is sparse and scales with the number of curves and surfaces in curve-networks and solids, respectively, and can be efficiently fed to existing image and graph convolution layers.
- We propose a novel hybrid architecture which comprises of an image CNN, and a hierarchical graph-neural network which is computationally efficient and can handle our representation.
- We create and release two related labeled datasets: WireMNIST and SolidMNIST, which capture variations in both geometry and topology of 2D curve-networks and 3D solids, respectively.
- We show applications of our representation on three tasks: classification, and self-supervised shape retrieval, pointcloud reconstruction and clustering. We leave generation of curve-networks and solids for future work, but our input representation composed of grids and graphs has high potential for these applications by coupling existing image and graph decoders [36, 23, 25, 33].

2 Preliminaries and Related Work

We first review some preliminaries related to 2D and 3D modeling with parametric curves and surfaces, and then review related work.

Curve-Networks and Solids Vector graphics are scale invariant representations which possess a wide range of benefits including ease of editability, concise representation, and resolution independence. SVG is the most popular standard for vector graphics. The fundamental primitive in SVGs are “paths” composed of a set of connected primitives including line segments, arcs, and non-rational Bézier curves. Paths can further be connected to other paths forming curve-networks.

In 3D design, a surface refers to a geometrical description of an object’s boundary without considering topological information. A surface is typically represented using parametric representations of

primitives such as planes, cylinders, spheres, toroids or more generally NURBS surfaces. A single surface is often not sufficient to model complex shapes, for e.g., since every NURBS surface is homeomorphic to a rectangle. Furthermore, a basic requirement in computer-aided design (CAD) is to represent an object unambiguously by not only describing its surface boundary, but also orienting it consistently, and ensuring accurate control over tolerance of errors and geometric continuity among different surfaces. This requires a notion of not just geometric definition, but topology related to how various surfaces are connected to each other and oriented is needed. To achieve these requirements, B-reps which encode both geometric and topological information were introduced [28]. B-reps include three main topological entities: faces which represent bounded portions of parametric surfaces, edges which represent bounded segments of parametric curves, and vertices which represent points. Additional topological entities are also used to define the adjacency relationships in the structure including shells, loops and lumps, see [29, 18] for details. A rich set of geometric and topological operations can be performed with such a data structure. Specifically, one can perform basic operations like trimming a surface by defining a closed curve in the parameter domain [5], as well as higher level operations such as lofting, extrusion, chamfering, filleting and drafting [20] (Ch. 10). The complex B-rep datastructure however, is difficult to feed into neural networks as surveyed by Babic et al. [2] where several classic machine learning methods for feature classification on B-reps are discussed.

Datasets. Large data collections that are challenging enough, yet easily accessible [6] are vital to encourage research in a domain. Some labeled datasets for curve-networks include Eitz et al. [9], which has 20,000 labeled freeform sketches, and the Google Quickdraw dataset [13] which has 50 million labeled doodles in 345 categories in vector and raster format. Quite recently, Han et al. [14] proposed a wireframe dataset of three-view line drawings for spatial reasoning tasks. Datasets for solid models are particularly limited. The ABC dataset [17] includes a large set of parametric solids, however, it requires significant cleaning up to remove duplicates, does not contain objects of specific categories, and is unlabeled. The machining feature dataset [34] is a labeled synthetic dataset of 1000 CAD models to recognize machining features for CAD applications. The models in each class are topologically identical, which makes it less challenging.

Deep Parametric Shape Processing. There is a recent interest in the machine learning community in topics surrounding parametric shapes, particularly related to 2D vector graphics in the context of font design. Ha and Eck [13] learnt from vector line drawings by converting them into polylines for sketch generation. Lopes et al. [19] generated SVG commands from rasterized images of fonts using a deep variational autoencoder. More recently, Wang et al. [32] used a Generative Adversarial Network to design fonts by learning mappings between font attributes and rasterized images. Modern deep learning approaches that directly work on parametric surfaces and solid representations are limited. Zhang et al. [34] classified voxelized solid models using a 3D CNN. Gao et al. [10] reconstructed B-splines control of 2D and 3D splines from images with a recurrent neural network. Their method is concerned with reconstruction rather than feature extraction. Moreover, the topology of shapes is not explicitly considered which is important in solid representations made of multiple surfaces. Recently, Smirnov et al. [27] proposed a framework for generating networks of Bézier curves, where the topology is provided by predefined templates. While we leave reconstruction and generation for future work, our input representation has high potential for these applications since we can consider a wide range of topologies using the graph representation, and differential properties of the input shapes can be incorporated to improve reconstruction quality [3]. Closely related to our consideration of geometry as regular grids or images are works by Gu et al. [12] which parametrized arbitrary meshes into a 2D regular grid for compression and resampling, Sinha et al. [26], which parametrized meshes globally as images to apply CNNs, Groueix et al. [11] where the parametrization of pointclouds itself is learnt, and Kawasaki et al. [15] where surface fairing was achieved by smoothing the normal map. Different from these works, we deal with multiple curves or surfaces with given parametrizations, that are stitched together to form complex shapes. In summary, recent deep learning application to curve-networks and solids has focused on conversion to other formats, or made simplifying assumptions to avoid modeling the topology, while in this work, we aim to explicitly include topology information and treat the geometry as 1/2-manifolds. By this, we can not only extract more representative features from the actual geometry of the shape, but also reduce the compute and memory footprint.

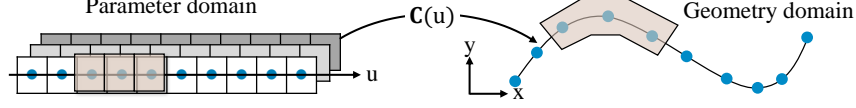


Figure 1: Representation of curve features in the parameter domain. A local neighborhood in the parameter domain corresponds to a local neighborhood in the geometry domain.

3 Method

3.1 Input representation

Given a curve network in 2D, or a solid model in 3D as input, our goal is to convert it into a representation that can easily and efficiently work with existing neural network architectures. It is highly preferable for the input representation to retain geometric and topological information and be as close as possible to the native representation. This rules out straightforward lossy, methods like triangle mesh tessellation, or point cloud sampling which ignore the topology.

2D case We first consider the case where we have a curve-network as input. Consider a parametric curve $C(u)$ in the curve network, which is a map from an interval $[u_{\min}, u_{\max}] \in \mathbb{R}$, the parameter domain, to the geometry domain \mathbb{R}^2 . The curve could be parameterized in any way including primitives such as lines, arcs, or freeform curves like Bézier or NURBS curves; we only expect that an interface is available to evaluate the curve and optionally, its first order derivative. Our main idea, similar to Kawasaki et al. [15] is to represent the geometry of the curve by discretizing its parameter domain as a regular 1D grid by a uniform step size $\delta u = \frac{u_{\max} - u_{\min}}{M-1}$, where M is the number of chosen samples, as shown in Figure 1. At each of the discretized points in the parameter domain u_k , we can attach a set of features evaluated from the curve, e.g., absolute point coordinates $C(u_k)$, and the unit normal vector $\frac{dC}{du}(u_k)^\perp$ (where \perp refers to a 90° CCW 2D rotation) as features. We create an edge-connectivity graph $G_C(V_C, E_C)$, where the vertices V_C correspond to each of the curves, and there is an edge in E_C between a pair of curves if they are directly connected to each other.

3D case In the case of a 3D solid, we have a set surfaces for each face of the solid. As before, we consider a parametric surface $S(u, v)$ which is a map from a 2D interval $[u_{\min}, u_{\max}] \times [v_{\min}, v_{\max}] \in \mathbb{R}^2$, the parameter domain, to the geometry domain \mathbb{R}^3 . We then discretize the parameter domain into a regular 2D grid of samples with step sizes $\delta u = \frac{u_{\max} - u_{\min}}{M-1}$, and $\delta v = \frac{v_{\max} - v_{\min}}{N-1}$, where M and N are the number of samples along each dimension, as shown in Figure 2. At each of these grid points indexed by (k, l) , we attach the following local features encoding the geometry of the surface: (1) 3D absolute point position $S(u_k, v_l)$. (2) Optionally, the 3D absolute surface normal $\frac{S_u(u_k, v_l) \times S_v(u_k, v_l)}{\|S_u(u_k, v_l) \times S_v(u_k, v_l)\|}$. The normal direction is flipped if the surface orientation is reversed compared to the face orientation. (3) Trimming mask with 1 and 0 representing samples that are inside and outside the surface’s trimming boundary loop, respectively. We use a simple face-adjacency graph derived from the B-rep of the solid model, $G_S(V_S, E_S)$ to model the topology, where the vertices V_S represent the surfaces in the solid model, while

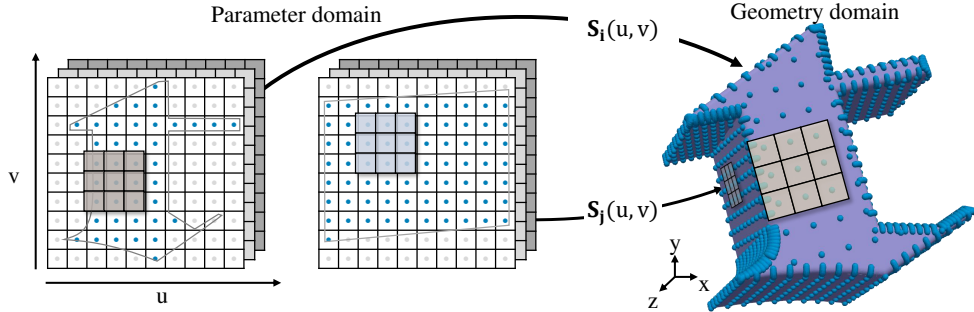
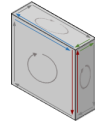


Figure 2: Representation of multiple surface features of a solid as regular parameter domain grids. We visualize samples outside of the trimming curve in light grey.

the edges E_S encode the connectivity between the faces which together form the complete solid object. This can be easily built by iterating through the halfedges of the B-rep and associating the face incident with each halfedge with that of its twin halfedge (see inset figure). While face adjacency is only a small subset of the rich topological information available in the B-rep, it is still sufficient to capture global information about a shape, as we show later in the experiments. Moreover, the graph representation could be extended in the future to include more topological information if necessary.

All features are computed after normalization of each curve-network and solid such that the largest extent of its bounding box is of size 2 and centered at origin, and the interval of parameter domain of each curve/surface snugly fits around the geometric boundary. We discuss more about feature computation in Appendix A. We set $M=N=10$ in all experiments throughout the paper. This is not a technical restriction, rather it is convenient to form minibatches of features. A fixed step size is sufficient when the mapping between parameter and geometry domains are roughly uniform. In the case of extreme parameterizations with high stretching, the sampling might miss out areas on geometry. For such scenarios, it is possible to derive a step size which guarantees an upper-bound on the distance between samples [35]. We do not take such an approach in this work, as special care needs to be taken during mini-batch construction due to arbitrary grid dimensions, and such extreme parameterizations are uncommon in modelling.

3.2 Advantages

There are several advantages of this representation: (1) Evaluating the curve/surface at a set of parameters is fast, e.g. using polynomial evaluation techniques like Horner’s method or forward differences [21], and the adjacency queries required for building the edge/face-adjacency graph take only constant time complexity with the B-rep datastructure. (2) The representation is largely invariant to the exact representation of the curve/surface equation. For example, the representation does not change when a curve is modified through degree elevation, knot insertion, etc. In contrast, the raw representation of a curve will appear to have changed significantly. (3) The 1D and 2D structured grid of features is easy to handle compared to unstructured representations such as pointclouds or sequential data. The regular 1D/2D grids representing curves/surfaces can be conveniently fed to convolutional layers for feature extraction, while the edge/face-adjacency graph representation can be fed to graph convolution layers. (4) A local neighborhood in the parameter domain corresponds to a local neighborhood in geometry domain of the curve/surface, hence convolutions in the parameter domain approximate convolutions on the curve/surface manifold [4]. (5) The structured grid of samples that we generate for curves and surfaces, is to a large extent invariant to common reparametrizations like knot refinement and degree elevation, and can be made invariant to parametrization reversals and transposes by applying line and square-symmetry group transformations to the uv-grid for augmentation. We explain this in more detail in Appendix B. (6) Finally, this representation can be converted back to the original curve-network or solid: individual curves/surfaces can be obtained by fitting since we know the parameters associated with the uv-grid samples, and the global shape can be obtained with the topological information in the edge/face-adjacency graph.

3.3 Network Architecture

With this representation, our idea is to perform image convolutions with shared weights on the uv-grids, which is equivalent to performing discrete curve/surface convolutions, to obtain local curve/surface features, and aggregate global features of the entire curve-network/solid by applying graph convolutions which leverage topology information as shown in Figure 3. Our CNN takes in uv-grids with 6 channels for curve-networks, and 7 channels for solids (as defined in Section 3.1), and is defined as $C(*, 64, 3) \rightarrow C(64, 128, 3) \rightarrow C(128, 256, 3) \rightarrow P_{AdpAvg}(1) \rightarrow FC(256, 64)$. Here, $C(i, o, k)$ is a convolutional layer (1D for curve-networks, and 2D for solids) with i input channels, o output channels, and kernel size k , $P_{AdpAvg}(n)$ is an adaptive average pooling layer which outputs a n (curve-network) or $n \times n$ (solids) sized feature map, and $FC(i, o)$ is a fully connected layer which takes an input in \mathbb{R}^i and maps it to \mathbb{R}^o . Both convolutional and fully-connected layers do not have biases, and include batch normalization and the LeakyReLU activation function. We use padding of size $\lfloor k/2 \rfloor$ in each convolutional layer to retain the spatial dimensions of the input. The output of our shared CNN is a set of features $h_v^{(1)}$, associated to each of the graph nodes $v \in V_*$, where V_* is a wildcard denoting either vertices V_C for curve-networks, or V_S for solids, and the superscript indexes into the graph layers $1 \dots K$.

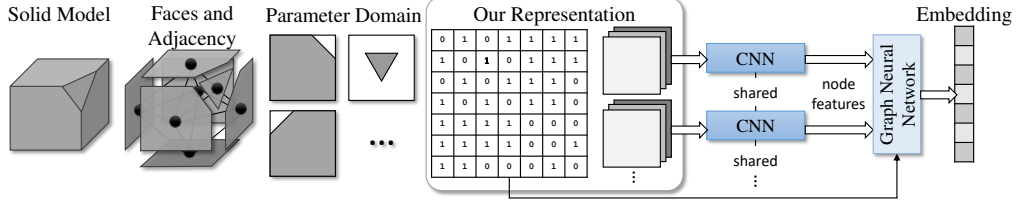


Figure 3: Network architecture. A solid model is represented by a set of regular uv-grid representing each face’s geometry by discretizing the parameter domain, and a graph that captures its topology with face-adjacency information. The uv-grids are passed through a shared CNN, and the features are further aggregated using a graph neural network to obtain the embeddings of the shape.

We use the Graph Isomorphism Network [31] to aggregate the features computed from the geometry of curves/surfaces while considering the topology captured in graphs G_C and G_S . Given the initial node features $h_v^{(1)}$ that we obtained from the features of the individual curve/surface obtained by 1D/2D convolutions, we recursively update the node features h_v^k in graph layer k , by aggregating the neighborhood node features from the previous layer $h_u^{(k-1)}$ with $u \in \mathcal{N}(v)$:

$$h_v^{(k)} = \text{MLP}^{(k)} \left((1 + \epsilon^{(k)}) h_v^{(k-1)} + \sum_{u \in \mathcal{N}(v)} h_u^{(k-1)} \right), \quad (1)$$

where $\text{MLP}^{(k)}$ is a multi-layer perceptron with two fully connected layers $FC(64, 64) \rightarrow FC(64, 64)$, $\epsilon^{(k)}$ is a learnable parameter to distinguish the center nodes from the neighbors. We then take all hidden features $\{h_v^{(k)} \mid k \in 1 \dots K\}$ and apply an element-wise maxpooling operation on each of them to obtain hierarchical feature vectors from every graph layer $\{h^{(k)} \mid k \in 1 \dots K\}$, where $h^{(k)} = \text{maxpool}_{v \in V_*}(h_v^{(k)})$. These features are then linearly projected with learnt weights $w^{(k)}$ and biases $b^{(k)}$ into 128-dimensional vectors and summed to obtain a single output feature vector to obtain the final shape embedding:

$$H(G) = \sum_{k=1}^K w^{(k)} \cdot h^{(k)} + b^{(k)} \quad (2)$$

We find that considering hierarchical graph features leads to significantly better performance. Depending on downstream applications, we attach a non-linear classifier, or MLP to obtain latent representations as detailed in the next section.

4 Experiments

We now show qualitative and quantitative results on supervised and self-supervised tasks: classification, shape retrieval, and reconstruction. We use our labeled WireMNIST and SolidMNIST datasets for classification and reconstruction, and the ABC dataset [17] for shape retrieval and reconstruction. WireMNIST is a set of 2D B-spline curve-networks generated from system fonts and the Google Fonts collection including both upper and lower cases, while SolidMNIST is a set of 3D solid B-reps generated by randomly extruding and filleting these curve-networks, resulting in 26 (a–z) categories. Details about creating the data, splits and visualizations are provided in Appendix C. For the ABC dataset, we consider a 45,000 subset, after removing duplicate parts. This is split randomly into training, validation and test sets using a 60:20:20 ratio. Results are reported on the test set for classification and reconstruction experiments, and the entire dataset for the shape retrieval experiment, using the best parameters found on the validation set. The model is trained for 350 epochs using a batch size of 128 optimized using Adam [16] in all experiments.

4.1 Classification

We first show results for the problem of classifying shapes in the WireMNIST and SolidMNIST dataset in Table 1. Our model comprises of a non-linear classifier (2-layer MLP) appended to the

Table 1: Classification results

Dataset	Model	Accuracy (%)	#Parameters
WireMNIST	Ours w/o normals	97.127 ± 0.064	396,380
	Ours w/ normals	97.066 ± 0.143	396,956
	CNN (64×64 images)	97.225 ± 0.086	976,570
SolidMNIST	Ours w/o normals	96.568 ± 0.074	643,868
	Ours w/ normals	96.683 ± 0.528	645,596
	PointNet (1024 points)	95.942 ± 0.076	813,914

Table 2: Self-supervised experiments by reconstructing images and pointclouds. Reconstruction loss is MSE for WireMNIST, and chamfer distance multiplied by 10^3 for SolidMNIST and ABC datasets.

Dataset	Input	Output	Clustering (AMI)	Recon. Loss
WireMNIST	Image	Image	0.6359 ± 0.0065	0.1011 ± 0.0001
	Curves (ours)	Image	0.5527 ± 0.0053	0.1155 ± 0.0002
SolidMNIST	Pointcloud	Pointcloud	0.7882 ± 0.0108	2.7090 ± 0.0067
	Solid (ours)	Pointcloud	0.7868 ± 0.0209	5.1737 ± 0.7862
ABC	Pointcloud	Pointcloud	N/A	2.0642 ± 0.0222
	Solid (ours)	Pointcloud	N/A	6.4778 ± 0.4526

network in Figure 3. For WireMNIST, we consider a CNN encoder similar to Lopes et al. [19] as a baseline, while for SolidMNIST, we consider PointNet [7] trained on pointclouds sampled from the solid by tessellation as baseline. Results show that our method can compete with baselines while properly modelling the geometry and topology of curve-networks and solids. Furthermore, our network has lesser parameters than baselines due to the our sparse input representation as well as hybrid convolutional architecture.

4.2 Self-supervised Learning

Ideally, we would have to reconstruct the geometry and topology of curve-networks or solids to extract their unsupervised representation. The research problem of jointly reconstructing the topology of a graph with arbitrary number of nodes, along with spatial node features is left to future work. Instead, we reconstruct images of curve-networks and pointclouds of solids using existing decoder architectures to demonstrate the potential of our encoder to learn useful representations. We use a CNN+transposed-CNN [19] autoencoder which takes in images of rasterized curve-networks, and PointNet [7]+(2-layer) MLP autoencoder which takes in pointclouds sampled from tessellated solids as baselines, which essentially learn an identity mapping.

In the case of WireMNIST, we pass the curve-networks through our encoder defined in Section 3.1 to obtain latent embeddings. An image decoder from [19] is then used to reconstruct another image I , by minimizing the mean-squared loss between pixels in \hat{I} and I , where the ground-truth \hat{I} is obtained by rasterizing the curve-networks into 64×64 binary images. With SolidMNIST and ABC datasets, we pass the solid model to our encoder (Section 3.1) to obtain latent embeddings of the shape. A simple 2-layer MLP point decoder [1] is then used to generate the pointcloud P , based on the symmetric Chamfer distance: $d_{\text{Ch}}(P, \hat{P}) + d_{\text{Ch}}(\hat{P}, P)$, where $d_{\text{Ch}}(A, B) = \sum_{a \in A} \min_{b \in B} \|a - b\|_2$, where the ground-truth pointcloud \hat{P} is generated by sampling 1024 points from the input solids.

We compare our reconstruction results against the baseline autoencoders in terms of Chamfer loss on the test set in Table 2. We further evaluate the quality of the embeddings obtained in this experiment from the WireMNIST and SolidMNIST dataset by applying k-means clustering, where the centroids are initialized using K-means++, and k is chosen to be the number of classes in the dataset, and each cluster is used to predict labels. This is compared with the ground truth using the Adjusted Mutual Information (AMI) metric in Table 2. Finally, we show results of shape retrieval in Figure 4, where our solid-pointcloud autoencoder on the ABC dataset and 5 nearest neighbors are found in the latent space given a query shape. More visual reconstruction and retrieval results are provided

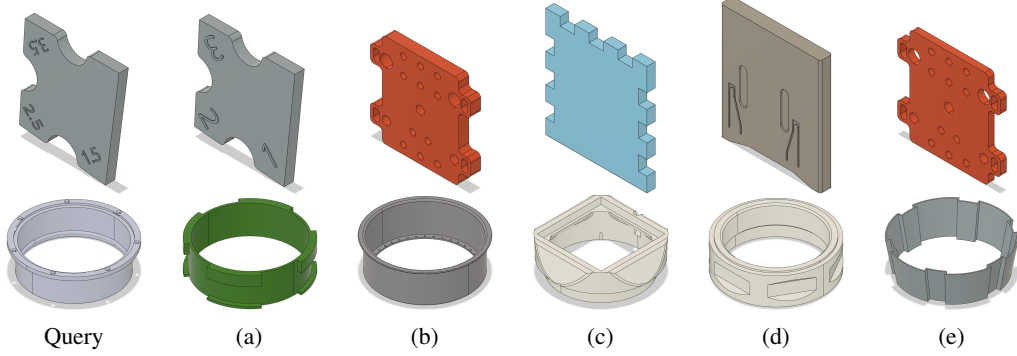


Figure 4: Shape retrieval on ABC Dataset. (a–e) Sorted nearest neighbors in latent space.

Table 3: Additional experiments. (a) Sensitivity to number of samples in the uv-grid. (b) Effect of reparametrization on classification w/ and w/o line/square symmetry augmentations.

(a)			(b)			
# Samples	Class. Acc.	Chamfer loss	Augmentation		Test Accuracy	
			Train	Test	WireMNIST	SolidMNIST
8×8	97.011	5.526	No	No	97.283	96.885
6×6	97.190	5.414	No	Yes	53.400	48.126
4×4	97.259	6.006	Yes	No	97.166	97.043
			Yes	Yes	97.222	97.074

in Appendix D. Our network is at a disadvantage compared to baselines as we are not learning an identity mapping. Despite that, we obtain good clustering and retrieval results.

4.3 Additional Experiments

Sensitivity to sampling step size We show in Table 3a how our method is robust to changes in sampling step size. It is apparent that the features captured at very sparse sampling steps are still sufficient to retain good accuracy in classification and reconstruction tasks. This shows the potential for making our input representation even sparse, or learning the step size as part of training in future.

Invariance to reparametrization We examine the invariance of our uv-grid representation to reparametrizations by randomly reversing, and transposing the parametrizations in the test set. We show in Table 3b that augmenting the training data with line- and square-symmetry transformations of uv-grids for curve-networks and solids, respectively, makes the model resilient to reparametrization.

5 Conclusion

We have presented a unified representation for curve-networks and solids, that can be leveraged by existing image and graph convolutional neural networks, and captures both the geometric and topological information. We accomplished this by discretizing the parameter domain of the geometry as regular 1D or 2D grids, and modelling the topology as a face-adjacency graph. Our representation is sparse and scales with the number of curves in a curve-network or faces in a solid compared to images or voxels which scale quadratically and cubically with resolution, or pointclouds or meshes which requires dense sampling to capture detail. We introduced a hybrid image and graph convolutional architecture that can process our representation efficiently and demonstrated its effectiveness on supervised and self-supervised tasks. Lastly, we created two new labeled datasets and baselines to encourage future research in this domain. We discuss limitations and future work in Appendix E. Our work opens up applications in various tasks where the input and output are both curve-networks and solids such as line drawing vectorization [24], font-design [32] and generation of unseen solids, where such a representation with geometric and topological aspects is necessary.

Broader Impact

The implications of this work are similar to any work that deals with 3D representations in the context of neural networks. We believe this work considers an important representation that has not been largely considered earlier, and can lead to a research trend where curve-networks and solid models are investigated more deeply by the machine learning community. We do not foresee any negative societal or ethical concerns that need to be particularly considered.

Acknowledgments and Disclosure of Funding

We thank Karl Willis for helping with processing the ABC dataset and proofreading, and Peter Bentley for helpful suggestions that improved the paper. This research was funded by Autodesk Inc.

References

- [1] P. Achlioptas, O. Diamanti, I. Mitliagkas, and L. Guibas. Learning representations and generative models for 3d point clouds. *arXiv preprint arXiv:1707.02392*, 2017.
- [2] B. Babic, N. Nesic, and Z. Miljkovic. A review of automated feature recognition with rule-based pattern recognition. *Computers in Industry*, 59(4):321 – 337, 2008. ISSN 0166-3615. doi: <https://doi.org/10.1016/j.compind.2007.09.001>. URL <http://www.sciencedirect.com/science/article/pii/S0166361507001327>.
- [3] J. Bednarik, S. Parashar, E. Gundogdu, M. Salzmann, and P. Fua. Shape reconstruction by learning differentiable surface representations, 2019.
- [4] M. M. Bronstein, J. Bruna, Y. LeCun, A. Szlam, and P. Vandergheynst. Geometric deep learning: Going beyond euclidean data. *IEEE Signal Processing Magazine*, 34(4):18–42, 2017.
- [5] M. S. Casale. Free-form solid modeling with trimmed surface patches. *IEEE Computer Graphics and Applications*, 7(1):33–43, 1987.
- [6] A. X. Chang, T. Funkhouser, L. Guibas, P. Hanrahan, Q. Huang, Z. Li, S. Savarese, M. Savva, S. Song, H. Su, J. Xiao, L. Yi, and F. Yu. ShapeNet: An Information-Rich 3D Model Repository. Technical Report arXiv:1512.03012 [cs.GR], Stanford University — Princeton University — Toyota Technological Institute at Chicago, 2015.
- [7] R. Q. Charles, H. Su, M. Kaichun, and L. J. Guibas. Pointnet: Deep learning on point sets for 3d classification and segmentation. In *2017 IEEE Conference on Computer Vision and Pattern Recognition (CVPR)*, pages 77–85, 2017.
- [8] T. S. Cohen and M. Welling. Group equivariant convolutional networks. In *Proceedings of the 33rd International Conference on International Conference on Machine Learning*, volume 48 of *ICML’16*, page 2990–2999. JMLR.org, 2016.
- [9] M. Eitz, J. Hays, and M. Alexa. How do humans sketch objects? *ACM Trans. Graph. (Proc. SIGGRAPH)*, 31(4):44:1–44:10, 2012.
- [10] J. Gao, C. Tang, V. Ganapathi-Subramanian, J. Huang, H. Su, and L. J. Guibas. Deepspline: Data-driven reconstruction of parametric curves and surfaces. *CoRR*, abs/1901.03781, 2019. URL <http://arxiv.org/abs/1901.03781>.
- [11] T. Groueix, M. Fisher, V. G. Kim, B. Russell, and M. Aubry. AtlasNet: A Papier-Mâché Approach to Learning 3D Surface Generation. In *Proceedings IEEE Conf. on Computer Vision and Pattern Recognition (CVPR)*, 2018.
- [12] X. Gu, S. J. Gortler, and H. Hoppe. Geometry images. *ACM Trans. Graph.*, 21(3):355–361, July 2002. ISSN 0730-0301. doi: 10.1145/566654.566589. URL <https://doi.org/10.1145/566654.566589>.
- [13] D. Ha and D. Eck. A neural representation of sketch drawings. *CoRR*, abs/1704.03477, 2017. URL <http://arxiv.org/abs/1704.03477>.
- [14] W. Han, S. Xiang, C. Liu, R. Wang, and C. Feng. SPARE3D: A dataset for SPATial REasoning on three-view line drawings. In *The IEEE Conference on Computer Vision and Pattern Recognition (CVPR)*, June 2020.

- [15] T. Kawasaki, P. K. Jayaraman, K. Shida, J. Zheng, and T. Maekawa. An image processing approach to feature-preserving b-spline surface fairing. *Computer-Aided Design*, 99:1 – 10, 2018. ISSN 0010-4485. doi: <https://doi.org/10.1016/j.cad.2018.01.003>. URL <http://www.sciencedirect.com/science/article/pii/S0010448518300411>.
- [16] D. P. Kingma and J. Ba. Adam: A method for stochastic optimization, 2014.
- [17] S. Koch, A. Matveev, Z. Jiang, F. Williams, A. Artemov, E. Burnaev, M. Alexa, D. Zorin, and D. Panozzo. Abc: A big cad model dataset for geometric deep learning. In *The IEEE Conference on Computer Vision and Pattern Recognition (CVPR)*, 2019.
- [18] S. H. Lee and K. Lee. Partial entity structure: A compact non-manifold boundary representation based on partial topological entities. In *Proceedings of the Sixth ACM Symposium on Solid Modeling and Applications, SMA '01*, page 159–170, New York, NY, USA, 2001. Association for Computing Machinery. ISBN 1581133669. doi: 10.1145/376957.376976. URL <https://doi.org/10.1145/376957.376976>.
- [19] R. G. Lopes, D. Ha, D. Eck, and J. Shlens. A learned representation for scalable vector graphics. *CoRR*, abs/1904.02632, 2019. URL <http://arxiv.org/abs/1904.02632>.
- [20] L. Piegl and W. Tiller. *The NURBS Book*. Springer-Verlag, New York, NY, USA, second edition, 1996.
- [21] T. W. Sederberg. "Computer Aided Geometric Design". BYU Faculty Publications, 2012. URL <https://scholarsarchive.byu.edu/facpub/1>.
- [22] T. W. Sederberg, J. Zheng, A. Bakenov, and A. Nasri. T-splines and t-nurccs. *ACM Trans. Graph.*, 22(3):477–484, 2003. ISSN 0730-0301. doi: 10.1145/882262.882295.
- [23] E. Shelhamer, J. Long, and T. Darrell. Fully convolutional networks for semantic segmentation. *IEEE Trans. Pattern Anal. Mach. Intell.*, 39(4):640–651, Apr. 2017. ISSN 0162-8828. doi: 10.1109/TPAMI.2016.2572683. URL <https://doi.org/10.1109/TPAMI.2016.2572683>.
- [24] E. Simo-Serra, S. Iizuka, K. Sasaki, and H. Ishikawa. Learning to simplify: Fully convolutional networks for rough sketch cleanup. *ACM Trans. Graph.*, 35(4), July 2016. ISSN 0730-0301. doi: 10.1145/2897824.2925972. URL <https://doi.org/10.1145/2897824.2925972>.
- [25] M. Simonovsky and N. Komodakis. Graphvae: Towards generation of small graphs using variational autoencoders. In V. Kůrková, Y. Manolopoulos, B. Hammer, L. Iliadis, and I. Maglogiannis, editors, *Artificial Neural Networks and Machine Learning – ICANN 2018*, pages 412–422, Cham, 2018. Springer International Publishing. ISBN 978-3-030-01418-6.
- [26] A. Sinha, J. Bai, and K. Ramani. Deep learning 3d shape surfaces using geometry images. In B. Leibe, J. Matas, N. Sebe, and M. Welling, editors, *Computer Vision – ECCV 2016*, pages 223–240, Cham, 2016. Springer International Publishing. ISBN 978-3-319-46466-4.
- [27] D. Smirnov, M. Fisher, V. G. Kim, R. Zhang, and J. Solomon. Deep parametric shape predictions using distance fields. *CoRR*, abs/1904.08921, 2019. URL <http://arxiv.org/abs/1904.08921>.
- [28] I. Stroud. *Boundary Representation Modelling Techniques*. Springer London, 2006. ISBN 9781846286162.
- [29] K. Weiler. *Topological Structures for Geometric Modeling*. Rensselaer Polytechnic Institute, 1986.
- [30] D. Worrall and G. Brostow. Cubenet: Equivariance to 3d rotation and translation. In V. Ferrari, M. Hebert, C. Sminchisescu, and Y. Weiss, editors, *Computer Vision – ECCV 2018*, pages 585–602. Springer International Publishing, 2018.
- [31] K. Xu, W. Hu, J. Leskovec, and S. Jegelka. How powerful are graph neural networks? In *International Conference on Learning Representations*, 2019. URL <https://openreview.net/forum?id=ryGs6iA5Km>.
- [32] Z. L. Yizhi Wang*, Yue Gao*. Attribute2font: Creating fonts you want from attributes. *ACM Trans. Graph.*, 2020.
- [33] J. You, R. Ying, X. Ren, W. Hamilton, and J. Leskovec. GraphRNN: Generating realistic graphs with deep auto-regressive models. In J. Dy and A. Krause, editors, *Proceedings of the 35th International Conference on Machine Learning*, volume 80 of *Proceedings of Machine Learning Research*, pages 5708–5717, Stockholm, Sweden, 10–15 Jul 2018. PMLR. URL <http://proceedings.mlr.press/v80/you18a.html>.

- [34] Z. Zhang, P. Jaiswal, and R. Rai. Featurenet: Machining feature recognition based on 3d convolution neural network. *Computer-Aided Design*, 101:12 – 22, 2018. ISSN 0010-4485. doi: <https://doi.org/10.1016/j.cad.2018.03.006>. URL <http://www.sciencedirect.com/science/article/pii/S0010448518301349>.
- [35] J. Zheng and T. W. Sederberg. Estimating tessellation parameter intervals for rational curves and surfaces. *ACM Trans. Graph.*, 19(1):56–77, 2000. doi: 10.1145/343002.343034. URL <https://doi.org/10.1145/343002.343034>.
- [36] S. Zheng, S. Jayasumana, B. Romera-Paredes, V. Vineet, Z. Su, D. Du, C. Huang, and P. H. S. Torr. Conditional random fields as recurrent neural networks. In *International Conference on Computer Vision (ICCV)*, 2015.

A Feature Computation and End-to-end Scenario

The input feature computation for our method is currently done offline prior to training. This is mainly because a CAD kernel is required to evaluate points, normals and the trimming mask of solids, as well as to compute tessellations for pointcloud generation in some experiments. In some scenarios, particularly with curve-networks, it is possible to make input feature computation part of the network. E.g. if we have a curve-network composed of cubic Bézier curves, then the evaluation of points and normals can be easily done as part of a `BezierSampler` layer inside the network end-to-end, since the Bézier curve evaluation is a differentiable function: $\mathbf{B}(u_k) = (1 - u_k)^3 \mathbf{P}_1 + 3(1 - u_k)^2 u_k \mathbf{P}_2 + 3(1 - u_k) u_k^2 \mathbf{P}_3 + u_k^3 \mathbf{P}_4$, where $\{u_k \mid k \in 1 \dots M\}$ are discrete values in the parameter domain and where \mathbf{P}_* are the control points. B-splines can be handled with some clever mini-batching since they can have an arbitrary number of control points and knots. Such a layer would be useful in scenarios where we want a non-uniform sampling scheme that is driven by optimizing for a given task, as opposed to a fixed step size in the parameter domain that we consider currently. We leave this exploration of learnable sampling and end-to-end training to future work.

B Invariance to Reparametrization

The structured grid of samples that we generate for curves and surfaces, is to a large extent invariant to common reparametrizations that do not change the shape. For e.g., during knot refinement and degree elevation, the parameterization and curve/surface geometry remains identical [20] and consequently the first derivatives also do not change. Hence our uv-grid representation is naturally invariant to these. Parametrization transposes (swapping u- and v-directions) and reversals (e.g., flipping u-direction) are handled as follows. With curves, we augment the data with the reversed version of the 1D grid (line-symmetry group). With surfaces, we have more cases to handle: swapping of u- and v- directions, reversing the u-, v-direction or both (square-symmetry group). Invariance to these is achieved by augmenting the data by rotating the grid by 90° , flipping it horizontally and vertically, in random. Alternatively, we could use convolutional layers that are invariant or equivariant to the symmetry group of a line (for curves) and square (for surfaces)—rotation by $k \frac{\pi}{2}$ for any integer $k \geq 0$, and reflections about each axis [8, 30]. Data augmentation for more complex reparametrizations, such as the Möbius transformation can be done prior to training, but we do not consider these reparametrizations in this work.

C WireMNIST and SolidMNIST Datasets

A publicly available, balanced, and labeled dataset is vital to serve as a standard benchmark for supervised tasks which are much easier to approach than unsupervised tasks on real-world datasets. To this end, we create “WireMNIST”, a labeled dataset of curve-networks, and “SolidMNIST”, a new labeled dataset for solid models. WireMNIST is a set of B-spline curve-networks generated from fonts collected from system fonts and the Google Fonts collection including both upper and lower cases (Figure 5a), while SolidMNIST is a set of solid models in B-rep representation generated from WireMNIST by extrusions.

For each character in the WireMNIST, we fill its interior with a trimmed planar sheet surface, see Figure 5a. We then treat the planar sheet as a profile surface on the XY-plane, and extrude it along a vector \mathbf{e} pointing upwards, see Figure 5b and Figure 5c. We define this vector such that its

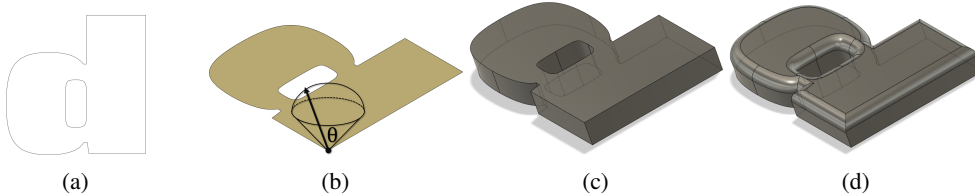


Figure 5: Running example of data generation. (a) 2D Curve-network going through boundary of the font face (WireMNIST). (b) Trimmed planar sheet filling the interior of the boundary. (c) Extrude. (d) Fillet edges of the topmost face (SolidMNIST).

head lies at a random point in the spherical cap situated along the z-axis to introduce variance in the extrusion direction. By sampling two random numbers ξ_1 and ξ_2 from a uniform distribution $U(0, 1)$, we can define the vector \mathbf{e} as: $\mathbf{e}_x = \sqrt{1 - \mathbf{e}_z^2} \cos(2\pi\xi_2)$, $\mathbf{e}_y = \sqrt{1 - \mathbf{e}_z^2} \sin(2\pi\xi_2)$, $\mathbf{e}_z = \xi_1(1 - \cos\theta) + \cos\theta$, where θ is the angle subtended by the spherical cap that we set to 45° . Furthermore, to break the symmetry of the shape across the XY-plane and introduce more complexity in the model, we identify the topmost face in the extruded solid and perform filleting by blending the edges with a constant radius 0.1, see Figure 5d. This introduces new curved faces in the model along the edges of the topmost face, and changes the topology as well. Choosing a suitable filleting radius is difficult since it depends on the topology of the face as well the thickness of the front face that was extruded which is not readily available. Hence, we attempt to fillet three times by successively reducing the filleting radius by 50%, and upon failure leave the extruded solid as such. After removing fonts that are non-English and symbols, we end up with 81343 train and 18971 test data split based on the font names, with an average of approximately 20 curves per curve-network in WireMNIST, and 33 faces per solid in SolidMNIST. We show a visual overview of the entire SolidMNIST dataset in Figure 6.

D Qualitative Results for Self-Supervised Experiments

We show qualitative results of pointcloud reconstructions from the experiments in Section 4 where we use our UVNet encoder and a pointcloud decoder in Figure 7. From the results, it is evident that the autoencoder is able to capture global features with a fair level of fidelity while reconstructing the pointclouds. This is particularly evident in SolidMNIST, and highlights the importance of such balanced and categorized datasets in this domain. The results, particularly for the "G" alphabet (row 1, column (e)), illustrate the need for encoders and decoders that can work with richly detailed solid models directly while considering both geometry and topology. More shape retrieval results on the ABC dataset are shown in Figure 8.

E Limitations and Future Work

Our method has some limitations which we plan to address in future work. First, we fix the sampling step size for each curve or surface regardless of its geometry. While this is convenient for batching the features, it can result in over-/under-sampling. Choosing the sampling step by analyzing the derivatives of surface [35, 15] or even learning it in a task-dependent manner would be an interesting extension. Second, we only consider a small subset of topological information available in a solid B-rep datastructure. While this is sufficient for the tasks we considered, we suspect that certain CAD specific applications for e.g., predicting the operations like extrusion or drafting that generated a given shape, and generating unseen solids will benefit from richer topology information. Third, our input representation captures the essence of the geometry, but ignores information about the exact geometric representation, e.g., plane vs. NURBS, which could be useful for some applications. Fourth, while our method is invariant to reparametrizations including reversals and transposes, it cannot handle situations when the same geometry is parametrized using a completely different uv-coordinate system. Finally, our solid dataset could benefit from richer augmentations such as random face splitting, merging, or slicing to make it more challenging and diverse. Other than addressing these limitations, we are interested in exploring generation of parametric curve-networks and solids using this representation in the future. We are also interested in extending our method to include more of the topological information from the B-rep datastructure, including explicit representation of vertices, halfedges, edges and faces, each with their own set of features. It is also worth investigating how our uv-grid representation can be applied to other sparse representations like subdivision surfaces, where the limit surface can be parametrized as a regular structure using the faces of the control mesh.

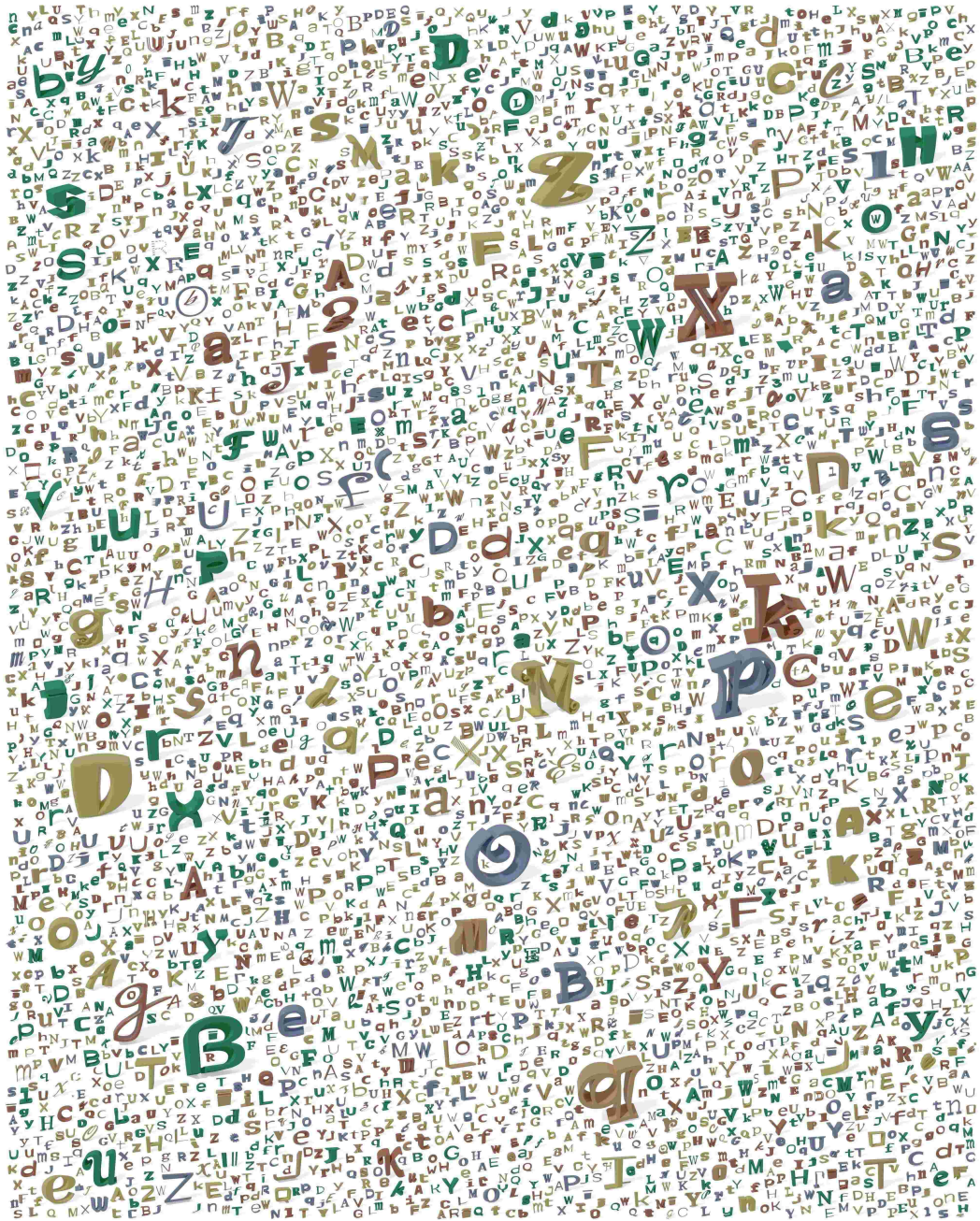


Figure 6: Visual overview of the SolidMNIST dataset.

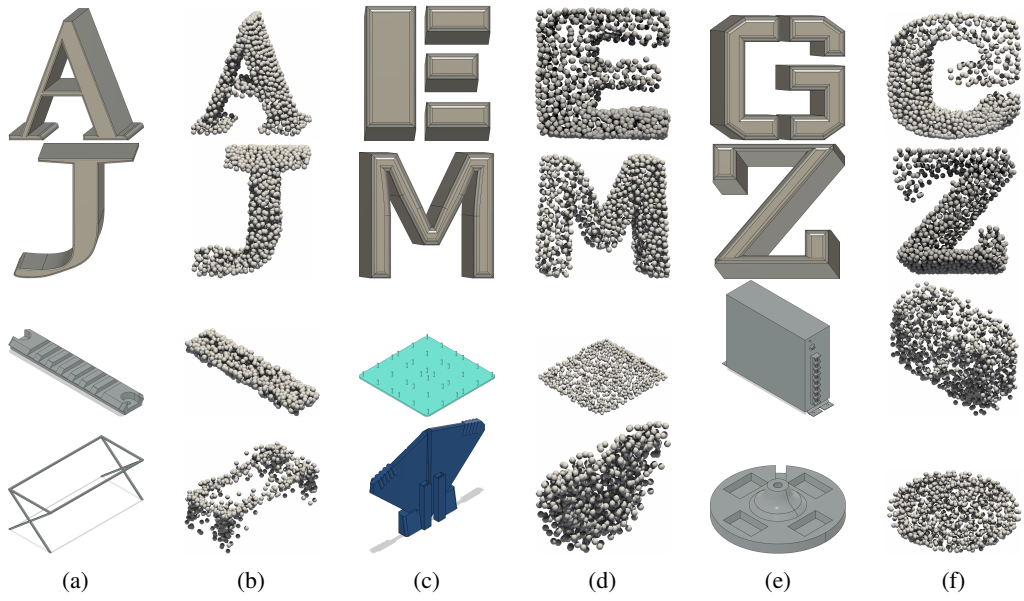


Figure 7: Pointcloud reconstruction results on the SolidMNIST (rows 1, 2) and ABC datasets (rows 3, 4). (a, c, e) Ground truth solid model. (b, d, f) Reconstructed pointclouds.

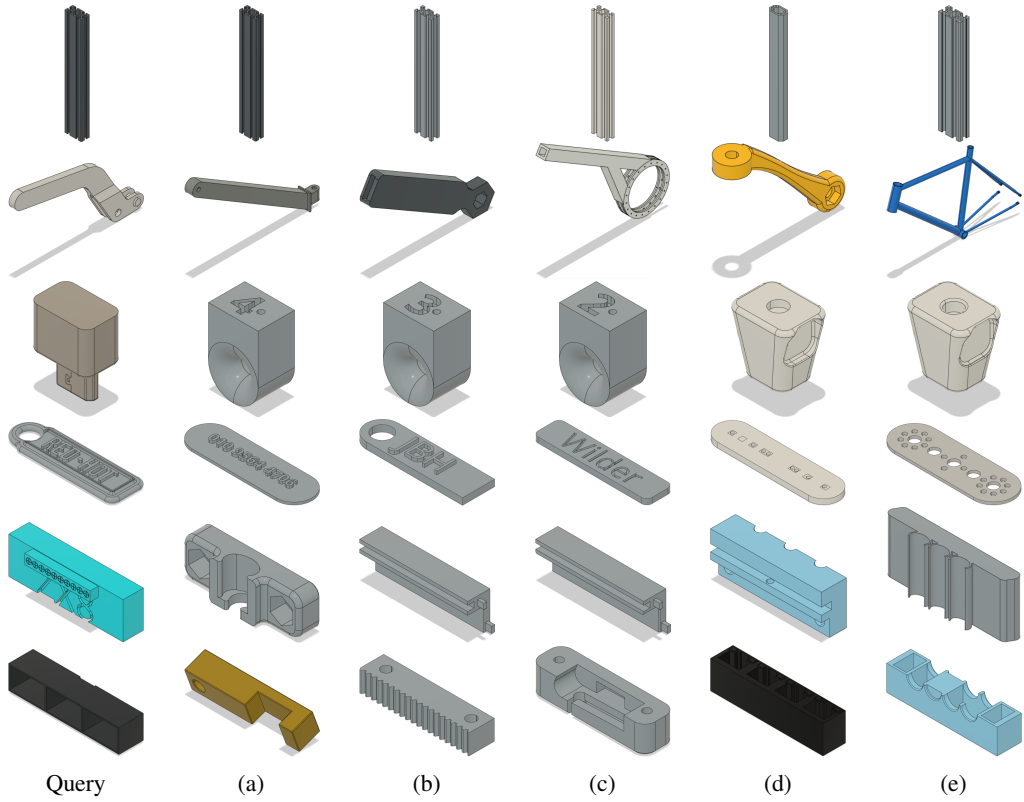


Figure 8: More shape retrieval results on the ABC dataset. Nearest neighbors to the query embedding are computed in latent space and shown sorted from (a) to (e).